AN ANALYSIS ON THE DYNAMICS OF A GAS BUBBLE IN A CENTRIFUGAL PUMP

Renzo H. G. Sabino, renzo_cs5@hotmail.com
Henrique Stel, stel.henrique@gmail.com
Dalton Bertoldi, daltonbertoldi@utfpr.edu.br
Moisés M. A. Neto, mneto@utfpr.edu.br
Rigoberto E. M. Morales, rmorales@utfpr.edu.br
NUEM/PPGEM/UTFPR, Av. Sete de Setembro 3165, CEP. 80230-901, Curitiba-PR-Brasil

Abstract. Electrical Centrifugal Pumps are quite common in the oil industry. Due to the despressurization during oil production , two-phase oil and gas mixtures flow through ESPs. Two-phase flow inside pump diffusers and impellers decreases its lift and efficiency. The technical literature presents a wide variety of studies about the influence of operational parameters, such as void fraction, rotor speed and inlet pressure on ESP global efficiency. Nevertheless, this influence is strictly related to the two-phase flow patterns. The present study evaluates two-phase flows inside pump diffusers and impellers by means of a single bubble flowing through the liquid bulk. An experimental apparatus was designed and built at the NUEM facilities. Original pump housings and impellers were replaced by transparent pieces in order to visualise bubbles flowing inside the pump. Bubble paths were followed both to define preference paths and to calculate bubble velocities. Additional CFD analysis yielded liquid velocities and static pressures through the pump impeller. An algebraic model, fed with numerical and experimental data, evaluated drag coefficient and drag force according to different experimental conditions.

Keywords: *ESP, two-phase flow, drag coefficient, drag force.*

1. INTRODUCTION

Offshore petroleum reservoirs are commonly submitted to high-pressure levels. The early years of well production are characterised by pressure levels that are high enough to lift the reservoir fluids all the way to the production facilities. After years of continuous operation, pressure levels decrease and artificial lift methods become necessary so as to keep production economically viable. Among the different techniques employed, the electrical submersible pump (ESP) is one of the most used worldwide.

ESPs are multistage pumps arranged in series. They can be installed inside a vertical or deviated well, and gas is produced together with the oil most of the time. It is acknowledged that the presence of dispersed gas inside the liquid bulk may cause significant performance degradation of centrifugal pumps (Gülich, 2010) leading to interventions to tune or change the existing ESP system. This is a major concern for petroleum companies since it is still unknown how a given ESP handles gas without high performance degradation or a complete pump shutdown (Estevam, 2002).

Lea and Bearden (1982) conducted one of the first works to study the performance degradation of ESPs operating with oil and gas. They experimentally investigated an oil well using a reduced number of pump stages, three types of ESPs and water-air and diesel-carbon dioxide as fluid models. They also analysed the degradation of performance with respect to the liquid flow rate, the gas void fraction and the pump speed. The authors also inspected the occurrence of surging, a phenomenon characterised by a large accumulation of gas inside the pump impeller channels that leads to a remarkable drop in the pump efficiency.

Following the work of Lea and Bearden (1982), some researchers (Estevam, 2002; Sachdeva; 1988; Cirilo, 1998; Barrios, 2007; Gamboa, 2008) analysed the performance of ESPs under gas-liquid admitting conditions. Particularly, Estevam (2002), Barrios (2007) and Gamboa (2008) used flow visualisation techniques in order to associate the performance trends to the behaviour of the gas inside the pump, including the situations under surging conditions.

Notwithstanding the fact that few works can provide a deep analysis on the movement of individual bubbles inside the liquid in an impeller channel (Murakami and Minemura, 1974a; Murakami and Minemura, 1974b; Minemura and Murakami, 1980), an analysis of the available literature shows that this problem is affected by a number of variables and therefore a great deal of information to bring further understanding of the phenomena involved with gas-liquid pumping is still required. For instance, useful information leading to the development of a suitable drag coefficient for bubble flows in such conditions is still lacking. The analysis of the forces acting on bubbles require the knowledge of factors such as the drag force and drag coefficient and thence to the understanding of the gas behaviour inside a pump as well as the comprehension about why the presence of gas degrades performance.

Having all this in mind, this work combines numerical and experimental techniques to evaluate the drag coefficient and the drag force according to different experimental conditions.

2. EXPERIMENTAL SETUP

The experimental setup was developed in order to allow the study of the dynamics of individual bubbles inside a centrifugal pump impeller. A scheme of the loop is presented in Fig. 1.

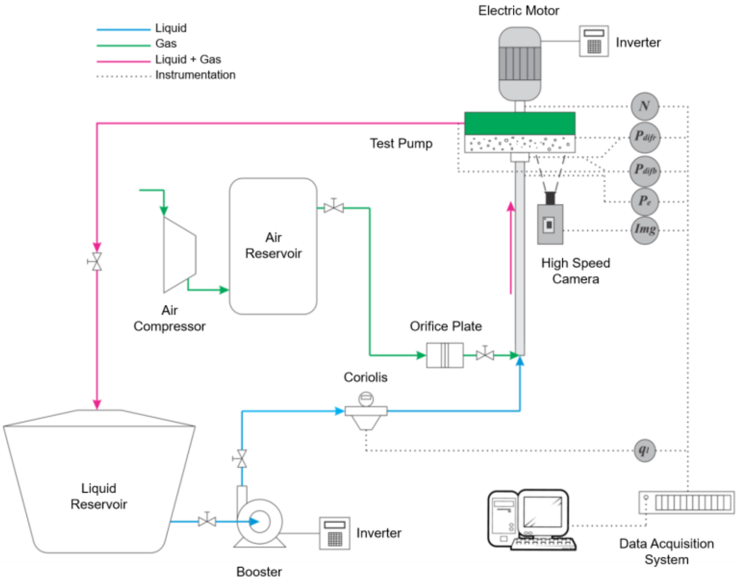

Figure 1. Experimental loop.

Water is pumped by a booster pump from the liquid reservoir through the loop. Its flow rate is measured by a Coriolis flowmeter., A 70-mm ID Plexiglas pipe with a L/D ratio of approximately 20 is adapted to the pump suction flange and is used to deliver a developed flow of liquid to the pump. Gas is inserted by means of an air compressor through a porous ceramic piece at the entrance section of the development pipe as indicated, and the L/D ratio of 20 proved to be sufficient for the bubbles to disperse and rearrange themselves inside the pipe up to the pump suction.

Whenever needed, the air flow rate is measured by means of an orifice plate in the air supply pipe prior to the bubbles insertion, whereas the volumetric flow rate can be corrected at the test pump suction flange through the entrance pressure, P_e. Two additional pressure transducers are used to collect the pressure differences across the whole pump, P_{difb}, and through the rotor, P_{difr}. Downstream the test pump, a globe valve is used to regulate the liquid flow rate. Just downstream this valve, another pipe carries the gas-liquid mixture back to the reservoir, where phases separate by gravity.

The test pump uses two radial impellers, a diffuser connecting those latter and a discharge volute. The original pump casing and the first impeller were replaced with transparent materials to allow visualisation of the bubbles flowing inside the first stage of the pump. This was accomplished by using a high speed camera focused orthogonally to the pump casing and the pump impeller, with the aid of a direct light source provided by a LED spot. An actual photograph of the system is shown in Fig. 2. Signals from all sensors and the booster pump frequency inverter, as well as the images from the high speed camera are controlled, processed and recorded by means of a dedicated data acquisition system as previously indicated in Fig. 1.

Images were acquired at 1000 fps. Due to the intake pipe positioning, the visualisation field was limited to only one 35-mm wide rotor channel section from the pump axis to the end of the rotor. Bubble velocities, at x and y directions, were obtained by image data evaluation.

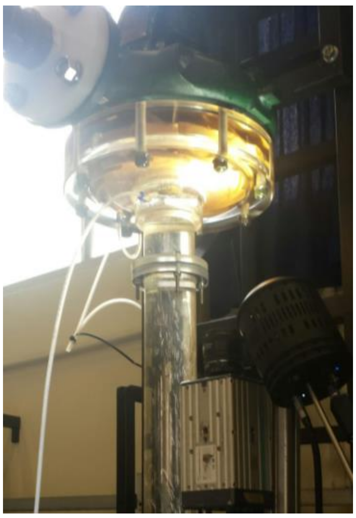

Figure 2. Photograph of the test pump with transparent casing, the high speed camera and the LED spot.

3. NUMERICAL PROCEDURE

As will be shown later, the drag coefficient will be evaluated by tracking the path of the bubbles inside the impeller channel and comparing the drag force exerted by the liquid over the bubble with the opposite pressure gradient created by the impeller. Numerical simulations of the single-phase flow of water inside the first stage of the test pump were performed in order to accomplish this task. It was assumed that the individual flow of a few small bubbles do not affect the flow field of water noticeably.

Numerical simulations were performed with the commercial package ANSYS® CFX® Release 14.5 (ANSYS, 2012). This computational fluid dynamics (CFD) software uses a finite volume method to solve the mass and momentum equations that govern the flow. Flow turbulence is modelled through Reynolds averaging and the standard k-ε model (Launder and Spalding, 1974).

For turbomachinery problems, the referred CFD software employs a multi-block technique in which each part of the pump, be it either static or rotating, comprises a separate domain. Then, information through domains is transferred by means of interface models. Figure 3 illustrates this concept for the present problem in, which the pump parts considered in the present analysis are an inlet pipe (static), the impeller (rotating), a vanned diffuser and an extension of the diffuser channel (both static).

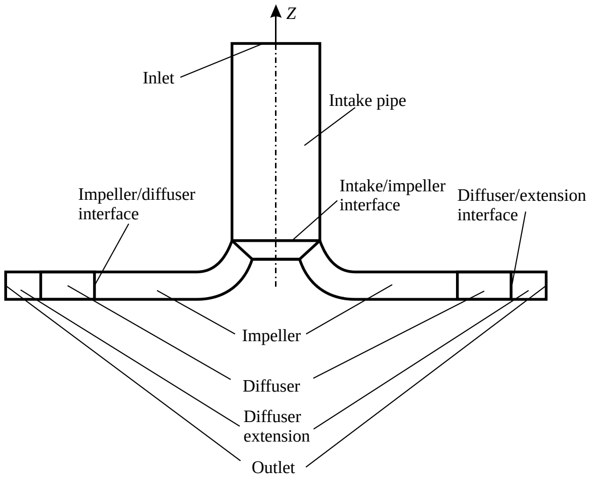

Figure 3. Schematic representation of the multi-block technique assumed for the present problem.

The numerical procedure used to model the rotation of the impeller with respect to the static parts can in general be accomplished in two ways. The first is to displace the rotor in small time steps, which is a more conservative and realistic approach and, in turn, very time consuming. An alternative is to keep a fixed reference position between the impeller and the static parts and account for its rotation by using source terms in the governing equations and proper interface models. This last approach results in much less time-consuming simulations and is the method used in this work. Complementary details about this procedure can be found in ANSYS (2012) and Stel *et al.* (2015).

The numerical grid used in the numerical simulations is constructed with hexahedral, body-fitted elements as shown in Fig. 4. Even though the whole 360º domain is shown, the blade number ratio between impeller (8 blades) and diffuser (12 vanes) was taken into account to simulate only 90º of each part with the help of periodicity conditions. More details on this procedure can also be found in ANSYS (2012) and Stel *et al.* (2015). After running mesh sensitivity tests, it was concluded that a total number of around 718,000 grid nodes is sufficient to give mesh independent results in the scope of the present study, where the impeller alone accounts for 620,000 nodes.

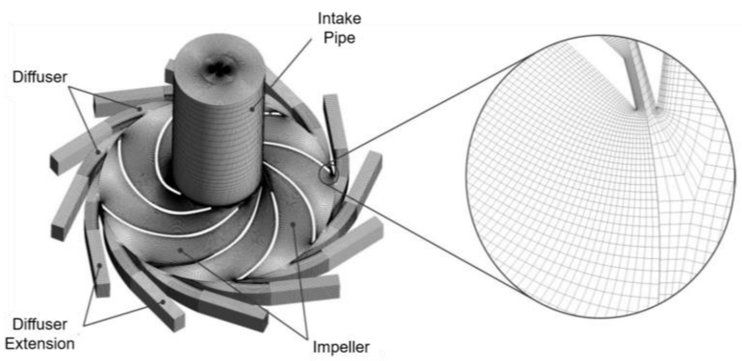

Figure 4. Numerical grid assumed for the present problem. The grid distribution near to the blade is show in detail.

One can notice from Figs. 3 and 4 that only the first stage of the pump is simulated, since it is the only stage for which experimental visualisation is possible. An intake pipe is assumed to make the inlet boundary condition far from the impeller eye. The inlet boundary condition was assumed as a 0 [Pa] total pressure (with respect to an ambient pressure of 1 [atm]), whilst a flow rate is imposed at the outlet sections of the diffuser extension. This last piece, by its turn, was used to keep the outlet condition far from the diffuser exit, as a way to avoid backward influence on the flow inside the impeller due to the fact that the second stage is disregarded. Walls are considered no-slip but smooth, that is, the effect of the wall roughness was neglected.

4. RESULTS AND DISCUSSION

Results for the bubble motion inside the pump impeller are presented in this section. The drag force resulting from a force balance on the bubble along its trajectory is also of particular interest. Results using the visualisation technique are obtained for rotation speeds from 100 to 220 rpm. Table 1 shows the operating conditions assumed for that purpose.

Table 1. Test conditions

Pump Speed [rpm]	Flow rate according to BEP [m^3/h]			
	0%	10%	20%	30%
100	3.18	3.50	3.82	–
110	3.50	3.85	4.20	–
120	3.82	4.20	4.58	4.96
170	5.41	5.95	6.49	–
220	7.00	7.70	8.40	–

4.1 Pump Performance.

Figure 5 shows the head curve versus flow rate experimentally obtained with the aforementioned loop with the pump commercial catalog curve and experimental data from Amaral (2007) for the same pump. All data is evaluated for a rotating speed of 612 rpm.

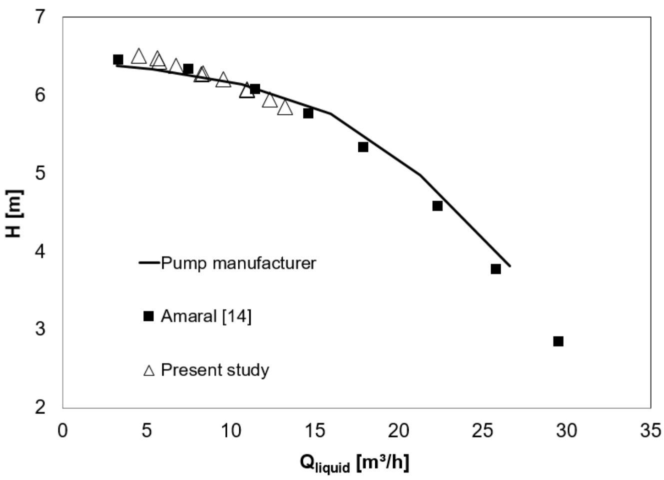

Figure 5. Head characteristic curve comparison.

Figure 5 shows that results agree well within the analysed range. Specifically for the first stage of the pump, the pressure rise obtained experimentally was compared with the numerical model described in section 3, and a good agreement was also observed.

4.2 Bubble Trajectory.

Figure 6 shows trajectories of several bubbles obtained by using the methodology described in section 2, for different rotating speeds. All data were acquired for liquid flow rates reduced to each rotating speed from the best efficiency point (BEP) flow rate at 1150 rpm assuming regular affinity laws. Bubble trajectory through the impeller channel is evaluated considering a non-inertial frame of reference that rotates with the impeller.

For 100 rpm, bubbles flow preferentially close to the blade suction side as shown in Fig. 6. However, this preferential path changes if the rotating speed is increased. As one can observe, at 170 and 220 rpm the bubbles tend to be displaced farther from the suction side in a slightly different behaviour in comparison with the 100 rpm case.

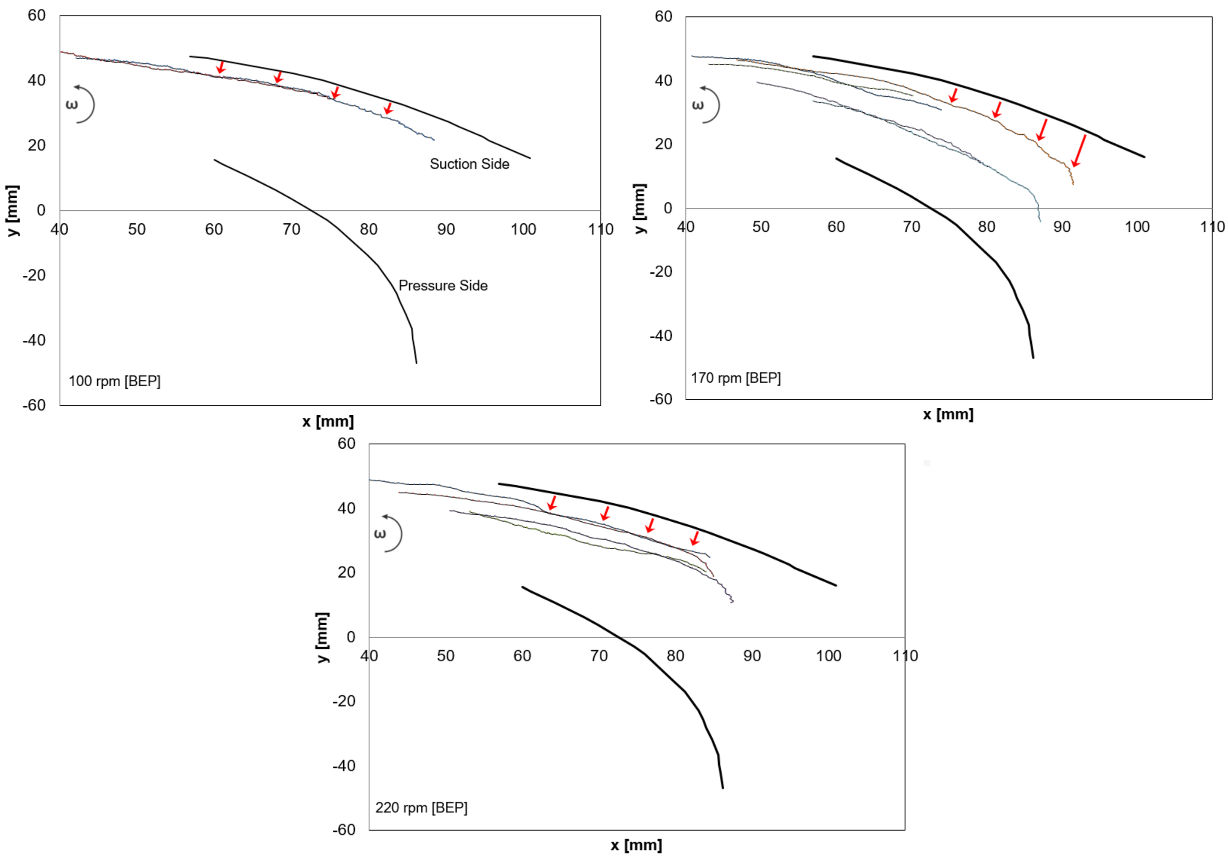

Figure 6. Bubble trajectories inside the impeller channel obtained by using the high speed camera for different rotating speeds.

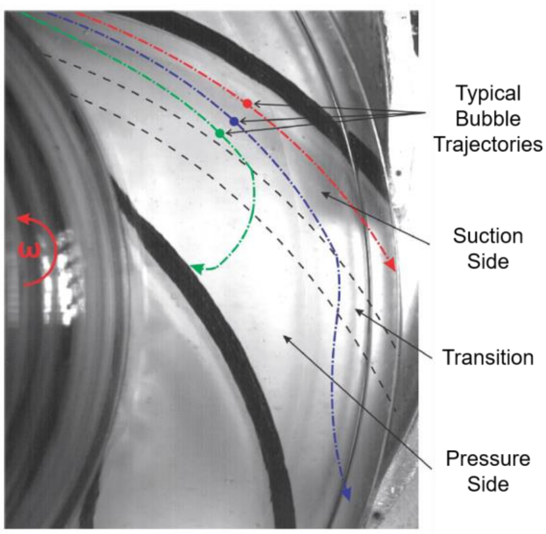

Figure 7. Illustration of the three basic trajectories of individual bubbles inside the impeller channel.

A careful inspection of the images obtained allowed the identification of trends for the motion of the bubbles. They generally consist of three basic types of trajectories, which are illustrated in Fig. 7. When a given bubble enters the impeller close to the suction side, it preferentially follows the blade curvature without sensible deviations downstream the exit. The red line depicts this path. If the bubble starts its motion inside the impeller farther from the suction side than the previous case, say, in the position denoted by the blue line, its trajectory tends to gradually deviate from the blade curvature. Close to the channel outlet, it can be suddenly pushed to the pressure side before exiting the impeller.

Otherwise, if the bubble enters the impeller even farther from the suction side (green line), it tends to be severely decelerated yet at the channel entrance. A displacement follows to the channel pressure side, and the bubble can be pushed back upstream to the impeller eye.

4.3 Drag Coefficient Estimation.

The methodology of Murakami and Minemura (1974a) was adopted in this article in order to estimate the drag coefficient consistent with the bubble motion inside the impeller. It is based on a force balance on a single bubble flowing through an impeller channel with constant relative velocity with respect to the liquid. The authors assumed an equilibrium between the drag and the pressure gradient forces acting in opposite directions on the bubble all along its path, whilst other interfacial forces are disregarded.

A more comprehensive balance force on a given bubble in a rotating frame of reference is given by Minemura and Murakami (1980) and can be expressed as:

$$\sum \vec{F} = \overrightarrow{f_d} + \overrightarrow{f_P} + \overrightarrow{f_{vm}} + \overrightarrow{f_B} + \overrightarrow{f_g} \quad , \tag{1}$$

where $\overrightarrow{f_d}$, $\overrightarrow{f_P}$, $\overrightarrow{f_{vm}}$, $\overrightarrow{f_B}$ and $\overrightarrow{f_g}$ represent the drag, the pressure gradient, the virtual mass, the gravity and the Basset forces. Expressions for these forces and information on how they impact the problem under analysis can be found in Minemura and Murakami (1980).

As discussed by Minemura and Murakami (1980), the two major forces acting on the bubble are indeed $\overrightarrow{f_d}$ and $\overrightarrow{f_P}$, and this is assumed in the present work. A scheme of the resulting balance is shown in Fig. 8, where an impeller channel is illustrated together with a non-inertial frame of reference and an arbitrary bubble path.

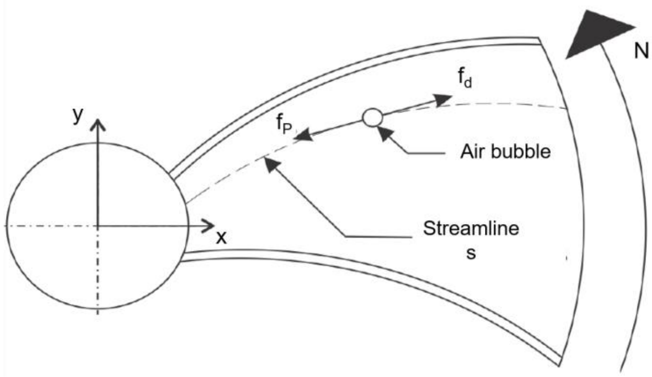

Figure 8. Force balance over an arbitrary air bubble.

The pressure gradient force, f_P , acts opposite to the bubble motion and arises from the pressure increase in the liquid provided by the impeller. It is proportional to the bubble volume and, when analysed over the bubble streamline path, is given by:

$$f_P = B_P \frac{\partial P}{\partial s} \tag{2}$$

where B_P is the bubble volume and $\partial P / \partial s$ is the pressure gradient over the streamline "*s*" at a given point.

By its turn, the drag force acts along the direction of the bubble path as a result from a difference between the bubble velocity and the surrounding continuum. The expression for this force is given as follows:

$$f_d = \frac{1}{2} C_d \rho_l \left(V_{sb} - V_{sl}\right)^2 \frac{\pi d_b^2}{4} \tag{3}$$

where C_d is the drag coefficient, ρ_l is the liquid density, V_{sb} and V_{sl} are the local velocity components of the bubble and the liquid in the direction of the streamline path and d_b is the bubble diameter.

Assuming that the drag and the pressure gradient forces are balanced along the trajectory, it follows that:

$$C_d = \frac{4}{3}\frac{d_b}{\rho_l\left(V_{sb} - V_{sl}\right)^2}\frac{\partial P}{\partial s} \tag{4}$$

Values of $\partial P/\partial s$ and V_{sl} cannot be evaluated using the present experimental loop, and were obtained from the numerical results. This is done by extracting the exact trajectory from the visualisation data in each case and using it later to calculate the values of $\partial P/\partial s$ and V_{sl} from the numerical results. The estimated drag coefficient, according to different bubble diameters, flow rates and rotating speeds, were compared to the Schiller and Naumann (1933) model:

$$C_d = \frac{24}{Re}\left(1+0.15Re^{0.687}\right) \tag{5}$$

where Re is the bubble Reynolds number based on its relative velocity.

4.4 Drag Coefficient as a Function of the Bubble Diameter.

Figure 9 shows a comparison of the estimated drag coefficient as a function of the bubble Reynolds number for different bubble diameters and three rotating speeds. It can be observed that C_d increases as the bubble diameter increases. However, this influence is expected to be negligible for high Reynolds numbers, where the drag coefficient tends to a constant, which seems to be the case here as well.

The C_d curve obtained from Eq. (4) for a rotating speed of 120 rpm and a bubble diameter equal to 0.63 mm proved to be the closest to the one obtained with Schiller and Naumann (1933) model. This seems to be consistent with the fact that smaller bubbles are more likely to keep a spherical shape, for which the Schiller and Naumann (1933) model is appropriate.

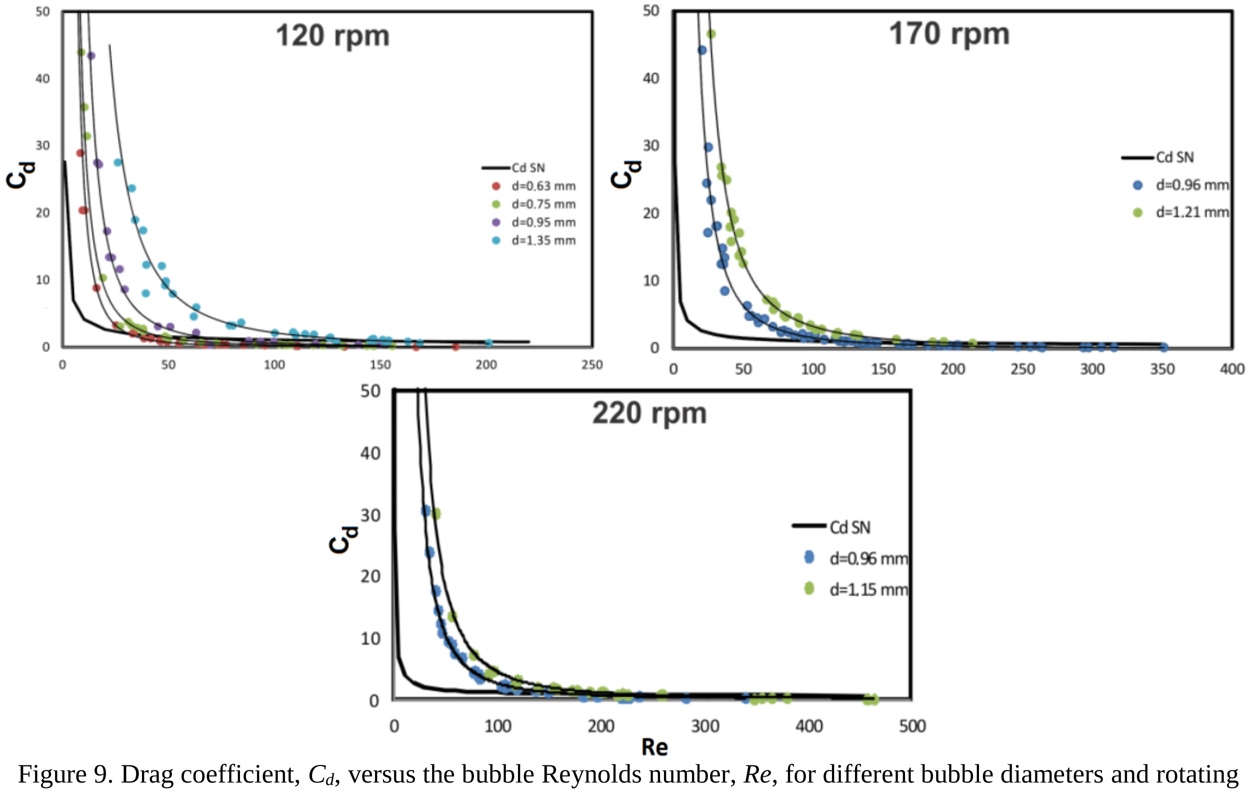

Figure 9. Drag coefficient, C_d, versus the bubble Reynolds number, Re, for different bubble diameters and rotating speeds.

4.5 Drag Coefficient as a Function of the Liquid Flow Rate.

Figure 10 shows the estimated drag coefficient as a function of the bubble Reynolds number for different liquid flow rates and two different rotating speeds. All cases were obtained for the same bubble diameter. As one can observe from Figs. 10 (a) and (b), the liquid flow rate has negligible influence on the C_d behaviour.

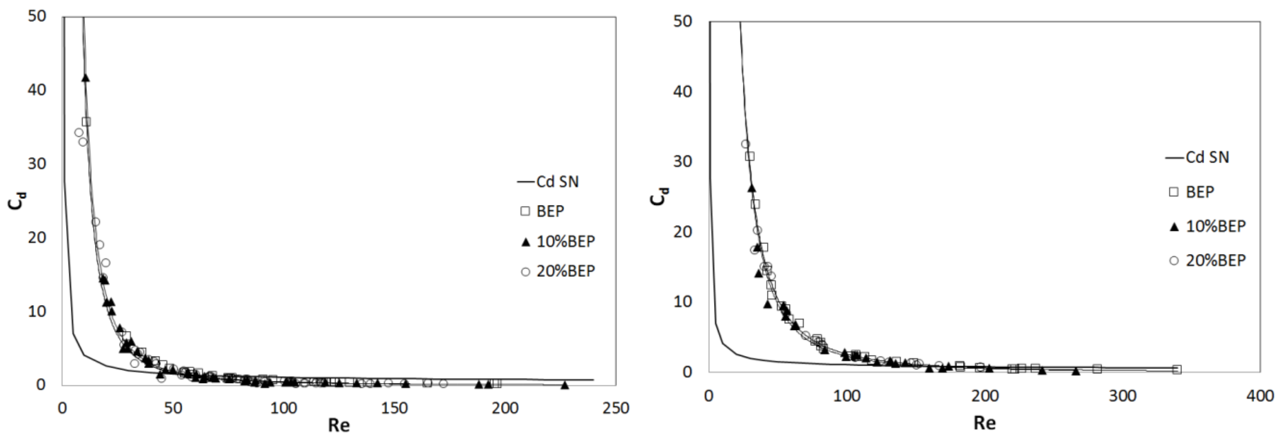

(a) (b)

Figure 10. Drag coefficient, C_d, versus the bubble Reynolds number, *Re*, for different liquid flow rates and two rotating speeds: (a) 100 rpm and (b) 220 rpm.

4.6 Drag Coefficient as a Function of the Rotating Speed.

Figure 11 compares the drag coefficient curve obtained for different rotating speeds, all for a flow rate consistent to the best efficiency point, for the same bubble diameter (namely 0.96 mm). It can be noticed that the drag coefficient increases with the impeller speed for a given Reynolds number. It should be noted, however, that the liquid flow rate at the best efficiency point also increases with the rotating speed, according to affinity laws. The actual effect of the rotating speed on the drag coefficient as well as a deeper investigation on both the experimental results and the numerical model used in this work are the subject of further works from the present group of authors.

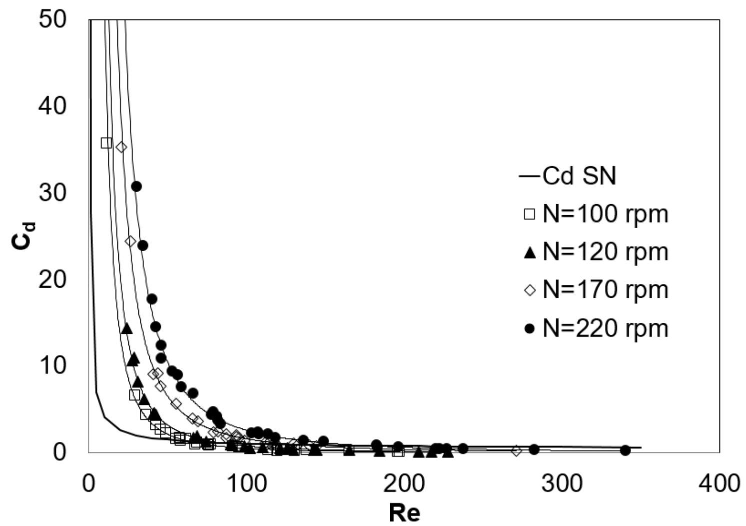

Figure 11. Drag coefficient, C_d, versus the bubble Reynolds number, *Re*, for different impeller rotating speeds.

5. CONCLUSIONS

This work presented an analysis of the dynamics of bubbles moving through a liquid phase inside a centrifugal pump impeller. High-speed visualisation (HSV) was used to observe the motion of bubbles inside the pump, whereas an algorithm was developed to compute the bubble trajectory, velocity and diameter for several operating conditions. A numerical model was also used to calculate the pressure and velocity flow fields inside the pump for liquid single-phase flows, which proved to be a useful tool to help obtaining estimations for the drag coefficients of the bubbles inside the impeller channels.

Distinct behaviours were identified for the motion of the bubbles inside the impeller, which are very sensitive to the position where the bubbles enter the impeller. In general, bubbles that flow close to the impeller suction side tend to follow the blade curvature, whilst the ones that enter the impeller at mid positions between blades may be severely deflected inside the hydraulic channel. Experimental results showed that the bubble diameter and the impeller rotating speed have a discernible effect on the drag coefficient, whereas negligible influence is observed with respect to the liquid flow rate. These influences and a more general description of the phenomenon are ongoing topics that the authors plan to examine in greater detail in the near future.

6. ACKNOWLEDGEMENTS

The authors acknowledge the financial support from CNPq, ANP and FINEP through the Human Resources Program to oil and gas segment PRH-ANP (PRH 10 - UTFPR) and from TE/CENPES/PETROBRAS.

7. REFERENCES

Amaral, G.D.L., 2007, "Modelagem do Escoamento Monofásico em Bomba Centrífuga Submersa Operando com Fluidos Viscosos, MS dissertation (in Portuguese), Universidade Estadual de Campinas, Campinas, Brazil.

ANSYS, 2012. ANSYS® Academic Research, Release 14.5, Help System, CFX Documentation, ANSYS, Inc.

Barrios, L. , 2007. Visualization and Modeling of Multiphase Performance inside an Electrical Submersible Pump, PhD dissertation, The University of Tulsa, Tulsa.

Cirilo, R., 1998. Air-Water Flow through Electric Submersible Pumps, MS thesis, The University of Tulsa, Tulsa.

Estevam, V. , 2002. Uma análise fenomenológica da operação de bomba centrífuga com escoamento bifásico, PhD thesis (in Portuguese), Faculdade de Engenharia Mecânica, Universidade Estadual de Campinas, Campinas, Brazil.

Gamboa, J., 2008. Prediction of the Transition in Two-Phase Performance of an Electrical Submersible Pump, PhD dissertation, The University of Tulsa, Tulsa.

Gülich, J.F., 2010. Centrifugal Pumps, second ed., Springer-Verlag, Berlin, Germany.

Launder, B.E. and Spalding, D.B., 1974. The numerical computation of turbulent flows, Computer Methods in Applied Mechanics and Engineering, Vol. 3, pp. 269-289.

Lea, J.F. and Bearden, J.L., 1982. Effect of Gaseous Fluids on Submersible Pump Performance, Journal of Petroleum Technology, Vol. 34, pp. 2922-2930.

Minemura, K. and Murakami, M., 1980. A Theoretical Study on Air Bubble Motion in a Centrifugal Pump Impeller, Journal of Fluids Engineering, Vol. 102, pp. 446-453.

Murakami, M. and Minemura, K., 1974a. Effects of Entrained Air on the Performance of a Centrifugal Pump (First Report, Performance and Flow Conditions), Bulletin of the JSME, Vol. 17.110, pp. 1047-1055.

Murakami, M. and Minemura, K., 1974b.Effects of Entrained Air on the Performance of a Centrifugal Pump (Second Report, Effects of Number of Blades), Bulletin of the JSME, Vol. 17.112, pp. 1286-1295.

Sachdeva, R., 1998. Two-Phase Flow through Electric Submersible Pumps, MS thesis, The University of Tulsa, Tulsa.

Schiller, L., Naumann, 1933. A.: VDI Zeits, 77, p. 318.

Stel, H., Sirino, T., Ponce, F.J., Chiva, S. and Morales, R.E.M, 2015. Numerical investigation of the flow in a multistage electric submersible pump, Journal of Petroleum Science and Engineering, Vol. 136, pp. 41-54.

8. RESPONSIBILITY NOTICE

The authors are the only responsible for the printed material included in this paper.